Journal of proteome research

Article

Changes of the Hepatic Proteome in Hepatitis B-Infected Mouse Model at Early Stages of Fibrosis

Daniela Spano, Flora Cimmino, Mario Capasso, Fulvio D'Angelo, Nicola Zambrano, Luigi Terracciano, and Achille Iolascon

J. Proteome Res., **2008**, 7 (7), 2642-2653• DOI: 10.1021/pr7006522 • Publication Date (Web): 22 May 2008

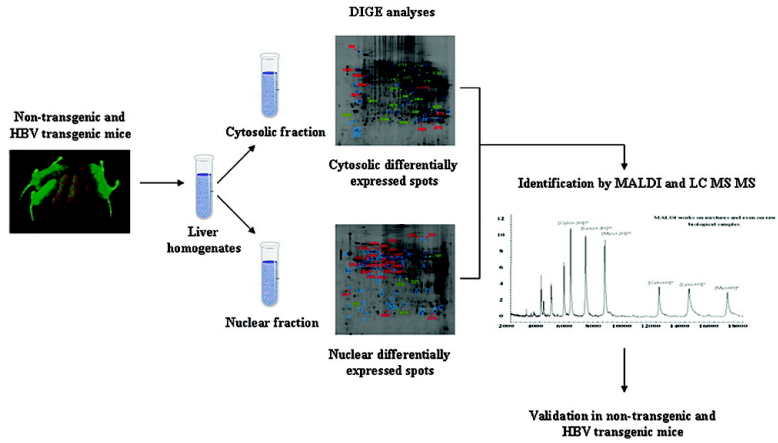

More About This Article

Additional resources and features associated with this article are available within the HTML version:

- Supporting Information
- Access to high resolution figures
- Links to articles and content related to this article
- Copyright permission to reproduce figures and/or text from this article

View the Full Text HTML

Journal of Proteome Research is published by the American Chemical Society.
1155 Sixteenth Street N.W., Washington, DC 20036

research articles Journal of proteome research

Changes of the Hepatic Proteome in Hepatitis B-Infected Mouse Model at Early Stages of Fibrosis

Daniela Spano,[†] Flora Cimmino,[†] Mario Capasso,[†] Fulvio D'Angelo,[†] Nicola Zambrano,[†,‡] Luigi Terracciano,[§,||] and Achille Iolascon*[,†,‡]

CEINGE Biotecnologie Avanzate, Napoli, Italy, Dipartimento di Biochimica e Biotecnologie Mediche, Università di Napoli Federico II, Napoli, Italy, Department of Pathology, University of Basel, Basel, Switzerland, and Dipartimento di Scienze per la Salute, Università del Molise, Campobasso, Italy

Received October 10, 2007

Liver fibrosis (LF) is the accumulation of extracellular matrix (ECM) proteins due to chronic liver injury. We used two-dimensional differential in-gel electrophoresis (2D-DIGE) to perform a comparative analysis of cytosolic and nuclear protein patterns of nontransgenic (NTg) and HBV transgenic (Tg) mice livers at early stages of fibrosis. We identified several candidate proteins, involved in a variety of pathways, which could be used as putative biomarkers for LF early detection.

Keywords: 2D-DIGE • HBV • transgenic animal • liver fibrosis • protein expression profile

Introduction

Liver fibrosis (LF) is the excessive accumulation of ECM proteins including collagens (predominantly collagen I and collagen III) that occurs in most types of chronic liver diseases.[1] Accumulation of ECM distorts the hepatic architecture by forming fibrous scar. The onset of LF is usually insidious, and most of the related morbidity and mortality occur after the development of cirrhosis.[2] In the majority of patients, progression to cirrhosis occurs after an interval of 15−20 years. Cirrhosis produces hepatocellular dysfunction and increased intrahepatic resistance to blood flow, which result in hepatic insufficiency and portal hypertension, respectively.[3] Moreover, liver cirrhosis predisposes to the formation of primary liver cancer or hepatocellular carcinoma (HCC).[4] The main causes of LF include chronic viral hepatitis B and C infections, alcohol abuse, drugs, nonalcoholic steatohepatitis, metabolic diseases, autoimmune attack on hepatocytes, or congenital abnormalities.[5] The wide geographic distribution and high prevalence of insults with the potential to cause LF suggest that LF and cirrhosis remain major causes of morbidity and mortality worldwide.[6]

Currently, liver biopsy is considered the gold-standard method for assessment of LF.[7] Histological examination is useful in identifying the underlying cause of liver disease and assessing the necroinflammatory grade and the stage of fibrosis. Liver biopsy is an invasive procedure, with pain and major complications occurring in 40% and 0.5% of patients, respectively.[8] Sampling error can occur, especially when small biopsies are analyzed. Furthermore, histological examination is prone to intra- and interobserver variation and does not predict disease progression.[9]

Recently, there has been significant progress in the development of proteomic approaches. Proteomics is defined as qualitative and quantitative comparison of proteomes under different conditions to further investigate biological processes. By allowing the large-scale analysis of proteins, proteomics represents a new experimental approach for identifying protein signatures and novel prognostic biomarkers of human disease, for discovering disease biology and mechanisms, new drug targets and much more. In particular, the characterization of liver proteome has become an essential step toward improvements in care for patients with liver diseases and will serve as the basis for current and future research. The number of liver proteins is very large and characterization of these proteins is complicated both by post-translational modifications and by splicing variants of gene products. Other key challenges include localization of proteins in the cell and protein−protein interactions. Proteomics offers hope for tackling this complexity and heralds significant advances in patient care.

The most powerful comparative proteomic approach is 2D-DIGE coupled with mass spectrometry (MS). DIGE technology[10] has improved the reproducibility, sensitivity and dynamic range of 2D-gel compared to the traditional 2D-PAGE and has allowed quantitative expression analysis. DIGE-based proteomics is however limited by the low identification rate of low-abundance proteins.

To identify potential biomarkers and/or protein expression signatures for early detection of LF, we analyzed the proteome of transgenic (Tg) mice, which overproduce the hepatitis B virus (HBV) large envelope polypeptide,[11] at early stages of LF. This animal model, among the two most commonly used models of experimental LF (elicited by carbon tetrachloride or thioacetamide intoxication, and bile duct ligation),[12,13] provides an opportunity for studying all biological steps characterizing liver

* To whom correspondence should be addressed. Achille Iolascon, Full Professor of Medical Genetics, Dipartimento di Biochimica e Biotecnologie Mediche, Universita'di Napoli Federico II; CEINGE Biotecnologie Avanzate, via Comunale Margherita 482, 80145-Napoli. Tel., +39 081 3737 897; fax, +39 081 3737 804; e-mail, iolascon@ceinge.unina.it.

[†] CEINGE Biotecnologie Avanzate.

[‡] Università di Napoli Federico II.

[§] University of Basel.

[||] Università del Molise.

10.1021/pr7006522 CCC: $40.75

Published on Web 05/22/2008

disease development in absence of chemical carcinogens or viruses, and mimics many of the pathological events that occur upon HBV infection in humans. Tgs accumulate toxic quantities of hepatitis B surface antigen (HBsAg) within the hepatocyte, develop severe, prolonged hepatocellular injury that initiates a programmed response within the liver, characterized by inflammation, fibrosis development, regenerative hyperplasia, transcriptional deregulation, and aneuploidy that inexorably progresses to neoplasia.[11,14–18]

In this study, our attention was focused on early stages of LF. We performed a systematic comparison of all protein changes that occur in nontransgenic (NTg) and Tg livers during the initial steps of LF using the DIGE technique. To improve low-abundance protein detection and 2-D electrophoresis resolution, we analyzed the proteome changes in two subcellular fractions enriched in either cytosolic or nuclear proteins. We detected significantly modulated expression of 141 (59 cytosolic and 82 nuclear) protein spots, identified 46 differentially expressed proteins from 53 picked-up spots, and validated the differential expression patterns of certain identified proteins by Western blotting (WB) analyses.

This study provides a large portfolio of targets useful for future investigations in molecular-marker discovery studies on large number of patients and functional assays. These studies should lead to the identification of markers that can be used to predict prognosis of LF and may provide further insight into the mechanisms of hepatic fibrogenesis.

Materials and Methods

Animals. C57BL/6J-Tg(Alb1HBV)44Bri/J (Tg) and C57BL/6J mouse strains were purchased from The Jackson Laboratory (Bar Harbor, ME). The animals were housed in an air-conditioned room (temperature, 21 ± 1 °C; relative humidity, 60 ± 10%) with the lights on from 2000 to 0800 h, in Plexiglas boxes (33 × 13 × 14 cm) with a metal top and sawdust as bedding. Pellet food (enriched standard diet, Mucedola, Settimo Milanese, Milan, Italy) and tap water were continuously available. The C57BL/6J-Tg(Alb1HBV)44Bri/J colony maintenance was performed crossing C57BL/6J-Tg(Alb1HBV)44Bri/J mice to C57BL/6J mice. The offspring genotyping was performed on mice tails' genomic DNA by PCR analysis according to manufacturer's protocols. Male nontransgenic littermates were utilized as controls to have the same genetic background as Tg mice. Six-month-old Tg and NTg males were sacrificed by cervical dislocation. At least three mice were used in each experiment, with the data subjected to statistical analysis. Livers were removed immediately after sacrifice, frozen in liquid nitrogen and stored at −80 °C until used.

Study protocols were in compliance with Italian law and institutional guidelines for use of laboratory animals.

Histopathological Examination. Male mice were killed at different times after birth (3, 6, 9 and 12 months). From all livers, parts were fixed, embedded in paraffin as previously described[19] and prepared for microscopic assessment using standards methods (hematoxylin-eosin and Sirius Red stainings). Necroinflammatory activity and fibrosis were assessed according to Ishak.[20] Liver sections were analyzed by an observer unaware of mice genotypes.

Cytosolic and Nuclear Extracts Preparation. The cytosolic and nuclear proteins extracts were performed as described[21] with some minor changes. Frozen liver tissues (1 g) from 6-month-old Tg and NTg males were homogenized on ice by a Potter type homogenizer in 10 mL of ice-cold lysis buffer (20 mM HEPES, pH 7.5, 250 mM sucrose, 1 mM EDTA, and 5 mM DTT) in the presence of 1× protease inhibitor cocktail (Complete Mini EDTA-free, Roche). Then the samples were centrifuged at 16 000*g* for 20 min at 4 °C and the obtained pellets were considered as the nuclear fraction, while the postnuclear supernatant (PNS) contained the cytosolic fraction and cell membranes.

The nuclear pellet was resuspended in 7 M urea, 2 M tiourea, 40 mM Tris-HCl, pH 8.5, 0.24% Triton X-100, and 4% CHAPS. After 30 min of incubation at room temperature, 20 mM spermine was added and the solution was incubated for 1 h at room temperature. The precipitated material was removed by ultracentrifugation at 100 000*g* for 45 min at 4 °C. The supernatant containing the nuclear fraction was saved in a clear tube.

The PNS was ultracentrifuged at 100 000*g* for 45 min at 4 °C. The obtained supernatant, considered as the cytosolic fraction, was solubilized in 7 M urea, 2 M tiourea, 40 mM Tris-HCl, and 4% CHAPS, and incubated for 30 min under agitation at room temperature.

Both the solubilized cytosolic and nuclear fractions were reduced by 5 mM tributylphosphine (TBP) for 90 min and were alkylated by 10 mM iodacetamide (IAA) for 90 min, in tubes wrapped in aluminum foil. After, the samples were precipitated for 90 min in a mix of acetone/methanol (8:1) at −20 °C and centrifuged at 13 400*g* for 30 min, at 4 °C. The pellets were air-dried and solubilized in 7 M urea, 2 M tiourea, 3% CHAPS, and 30 mM Tris-HCl . Protein concentrations were determined using the Bradford method (Bio-Rad).

Labeling of Cytosolic and Nuclear Extracts. The pH of the samples was adjusted to 8.5 with 0.1 M NaOH or HCl. Cytosolic and nuclear extracts (50 μg) from three different 6-month-old NTg and Tg males were labeled separately with 400 pmol of Cy3 and Cy5. A pool composed of equal amount of all samples of each cytosolic or nuclear extract was prepared and labeled with Cy2 to be used as a standard on all gels. Labeling reactions were performed on ice in the dark for 30 min and stopped with 1 mM free lysine (final concentration). Samples were mixed and the final volume was adjusted to 450 μL with 7 M urea, 2 M tiourea, and 3% CHAPS. Cytosolic and nuclear samples were supplemented, respectively, with 0.5% carrier ampholytes pH 3−10 (Bio-Rad, Segrate, Milan, Italy), pH 3−11 (GE Healthcare, Milan, Italy), and 1% bromophenol blue.

2-D Gel Electrophoresis, Imaging, and DIGE Analysis. IPG strips (length, 24 cm; thickness, 0.5 mm) (GE Healthcare), nonlinear pH gradient range 3−10 for cytosolic extracts and 3−11 for nuclear extracts, were passively rehydrated with 150 μg of tripartite-labeled sample (50 μg for each labeled sample and 50 μg internal standard), in the dark overnight. The nuclear extracts IEF was performed on nonlinear IPG strips, pH gradient range 3−11, because on these strips the resolution of protein spots was better than that obtained on nonlinear IPG strips, pH gradient range 3−10. IEF was performed using an Electrophoresis Unit (GE Healthcare) at 20 °C, with a maximum current setting of 50 μA/strip, in dark condition. IEF run conditions were the following: linear voltage up to 200 V in 1 h, up to 1000 V in 1 h, up to 1500 V in 1 h, up to 3500 V in 1 h, constant voltage to 3500 V for 3 h, linear voltage up to 5000 V in 1 h, constant voltage to 5000 V for 4 h, linear voltage up to 8000 V for 1 h, and constant voltage to 8000 V until the total product time × voltage applied was 76 000 Vh for each strip. The strips were equilibrated, loaded and run onto 24 cm × 20 cm 10% polyacrilamide gels as previously described.[21] The 2-D gels were scanned, and the images were analyzed as

previously described.[21] A total of 3500 spots/gel were detected using the DeCyder 5.0 image analysis software (GE Healthcare). Protein spots that showed a statistically significant Student's *t* test (p-value ≤ 0.075) for an increased or decreased expression level equal or above 1.75 were accepted as being differentially expressed between the extracts under comparison.

In-Gel Digestion and Peptide Extraction. For preparative purposes, IEF/SDS-PAGE was performed as described above using 1 mg of unlabeled cytosolic or nuclear proteins extracts. Preparative gels were fixed in 10% acetic acid/40% methanol solution for 12−16 h, stained using the universal staining methods of anionic dyes (Coomassie Colloidal Blue; Pierce) for 3 days, and destained in deionized H_2O. Protein spots of interest were manually excised from the gels and washed in 50 mM ammonium bicarbonate, pH 8.0, in 50% acetonitrile until completely destained. The gel pieces were resuspended in 50 mM ammonium bicarbonate, pH 8.0, containing 100 ng of trypsin, and incubated for 2 h at 4 °C and overnight at 37 °C. The supernatants containing the resulting peptide mixtures were removed and the gel pieces were re-extracted with acetonitrile. The two fractions were then collected and freeze-dried.

Mass Spectrometry Analysis and Protein Identification. 1. MALDI MS Analysis. MALDI mass spectra were recorded on an Applied Biosystem Voyager DE-PRO mass spectrometer equipped with a reflectron analyzer and used in delayed extraction mode. One microliter of peptide sample was mixed with an equal volume of α-cyano-4-hydroxycynnamic acid as matrix (10 mg/mL in 0.2% trifluor acetic acid (TFA) in 70% acetonitrile), applied to the metallic sample plate and air-dried. Mass calibration was performed using the standard mixture provided by the manufacturer. Mass signals were then used for database searching using the MASCOT peptide fingerprinting search program (Matrix Science, Boston, MA), available on the Internet.

2. LC-MS MS Analysis. The unknown protein spots from peptide mass fingerprinting were further analyzed by LC-MS MS using a Q-TOF Ultima hybrid mass spectrometer (Micromass, Waters) equipped with a Z-spray source and coupled online with a capillary chromatography system (CapLC, Waters). The peptide mixture (10 μL) was first loaded onto a reverse-phase trap-column (Waters) at 10 μL/min using 0.2% formic acid as eluent. The sample was then transferred to a C_{18} reverse-phase capillary column (75 μm × 20 mm) at a flow rate of 280 nL/min and fractionated using a linear gradient of running buffer B (0.2% formic acid in 95% acetonitrile) in running buffer A (0.2% formic acid in 5% acetonitrile) from 7% to 60% in 50 min. The mass spectrometer was set up in the data-dependent MS/MS mode to alternatively acquire a full scan (m/z acquisition range from 400 to 1600 Da/e) and a tandem mass spectrum (m/z acquisition range from 100 to 2000 Da/e). The three most intense peaks in any full scan were selected as precursor ions and fragmented by collision energy. Raw MS and MS/MS spectra were elaborated by the ProteinLynx software, provided by the manufacturers that generated a peak list containing all of the fragmentation data that was used for database searching using the MASCOT MS/MS ion search software for protein identification.

3. Protein Identification by Bioinformatic Tools. Raw data from nanoLC-ESI-MS/MS analyses were converted into a Mascot format text to identify proteins by means of a Mascot software version 2.1 in home, MatrixScience (Tonge, R. et al.).[10] The protein search both from nanoLC-ESI-MS/MS and MALDI MS analyses was governed by the following parameters: nonredundant protein sequence database (NCBInr −20061017 database with 4 051 787 sequences and 1 396 484 404 residues downloaded; Sprot- 50.9 database with 235 673 sequences and 86 495 188 residues downloaded); specificity of the proteolytic enzyme used for hydrolysis (trypsin); taxonomic category of the sample (*Mus musculus*); no protein molecular weight was considered; up to 1 missed cleavage; cysteines as *S*-carbamidomethylcysteines; unmodified N- and C-terminal ends; methionines both unmodified and oxidized; putative pyroGlu formation by Gln; precursor peptide maximum mass tolerance of 150 ppm and a maximum fragment mass tolerance of 100 ppm.

Data Mining. The identified proteins were classified according to DAVID 2.1 beta annotation system (http://david.abcc.ncifcrf.gov). This tool adopts the Fisher exact test to measure the protein-enrichment in annotation terms. A Fisher exact test $P = 0$ represents perfect enrichment. If the p-value is equal to or smaller than 0.05, a protein would be considered strongly enriched in the annotation categories. Functional Annotation Clustering integrates the same techniques of Kappa statistics to measure the degree of common proteins between two annotations, and fuzzy heuristic clustering to classify the groups of similar annotations according kappa values.[22] The heuristic partitioning procedure allows an object (protein) to participate in more than one cluster. The use of this method in grouping related proteins much better reflects the nature of biology in that a given protein may be associated with more than functional group of proteins. Two additional advancements included in this algorithm are (1) the automatic determination of the optimal numbers of clusters (K), and (2) the exclusion of members (proteins) that have weak relationships to other members.

WB Analyses. Twenty-five micrograms and fifty micrograms of cytosolic and nuclear extracts were loaded onto 8% or 12% polyacrilamide gels. The WB analyses were performed as previously described[21] using the following commercial primary antibodies: rabbit anti-Enolase (1:1000; Santa Cruz Biotechnology), rabbit anti-Sp1 (1:100; Santa Cruz Biotechnology), goat anti-LMβ (Lamin B) (1:100; Santa Cruz Biotechnology) antibodies.

Frozen liver tissues (1 g) from 6-month-old Tg and NTg males were homogenized on ice by a Potter type homogenizer in 10 mL of ice-cold RIPA lysis buffer (50 mM Tris-HCl, pH 8.0, 150 mM NaCl, 1% (v/v) Triton X-100, 0.1% SDS, and 10% (v/v) glycerol) in the presence of 1× protease inhibitor cocktail. Homogenates were vortexed for 15 min and centrifuged at 16 100g for 45 min at 4 °C. Supernatant was collected and assayed for protein content by BCA protein assay reagent (Pierce, Rockford, IL). The total protein extracts were frozen and stored at −80 °C until assayed.

Fifty micrograms of total protein extracts was loaded onto polyacrilamide gels and WB analyses were performed as previously described[21] using the following commercial primary antibodies: rat anti-GRP78 (78 kDa glucose-regulated protein) (1:100; Santa Cruz Biotechnology, Santa Cruz, CA), rabbit anti-PDI (Protein disulfide-isomerase) (1:100; Santa Cruz Biotechnology, Santa Cruz, CA), mouse anti-HMGB1 (High mobility group protein B1) (1:500; Abcam, Cambridge, U.K.), mouse anti-KRT18 (Keratin, type I cytoskeletal 18) (1:800; Sigma Aldrich, Milan, Italy), mouse anti-KRT8 (Keratin, type II cytoskeletal 8) (1:50; Progen), mouse anti-ALDH2 (Aldehyde Dehydrogenase 2 family, mitochondrial) (1:3000; Abnova Corporation), goat anti-PRDX1 (Peroxiredoxin-1) (1:25; Santa Cruz Biotechnology,

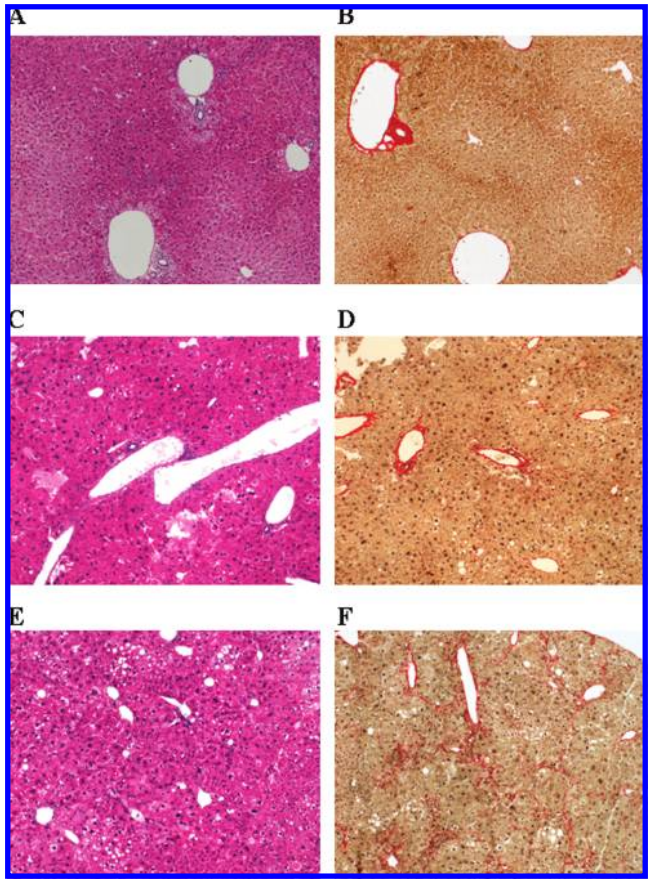

Figure 1. Histopathological examination. Liver sections of NTg (A, B), 6-month-old Tg (C, D) and 12-month-old Tg (E, F) were stained with hematoxylin-eosin (A, C, E) and Sirius Red (B, D, F). The fold magnification was ×10.

Santa Cruz, CA), rabbit anti-GRP94 (Tumor rejection antigen) (1:50; Santa Cruz Biotechnology, Santa Cruz, CA), rabbit anti-KRT8 phospho S73 (1:500; Abcam Cambridge, U.K.), mouse anti-KRT8 phospho S431 (2 μg/mL; Abcam Cambridge, U.K.), mouse anti-KRT18 phospho S33 (2 μg/mL; Abcam Cambridge, U.K.), rabbit anti-SOD (Superoxide Dismutase 1) (0.2 μg/mL; Abcam Cambridge, U.K.) antibodies. The secondary antibodies were the following: horseradish peroxidase (HRP)-conjugated anti-rat, anti-mouse, anti-rabbit and anti-goat antibodies (1: 10 000) (Santa Cruz Biotechnology). A rabbit anti-GAPDH antibody (1:1000; Cell Signaling Technology, Danvers, MA) was used as control for equal loading. Semiquantitative analyses of proteins expression were performed. The bands were quantified by densitometry to obtain an integral optical density (OD) value, which then was normalized with respect to the GAPDH value. Statistical analysis was performed using Student's *t* test. Differences of protein expression at *p*-value ≤ 0.05 were considered statistically significant.

Results

Histopathological Characterization of Liver. Histopathological examination was performed on NTg and Tg liver sections at different ages (3, 6, 9 and 12 months) to evaluate fibrosis staging and necroinflammatory grading. NTg sections did not exhibit any evidence of either necroinflammatory activity or of fibrosis at all examined times (Figure 1A,B).

Liver sections from Tg mice at 3 months showed a slight "ground-glass" appearance of the hepatocyte, without inflammation or fibrosis. By 6 months, there was an accumulation of eosinophilic granular bodies in the cytoplasm of many hepatocytes. Anisonucleosis, intralobular mononuclear cell infiltrates and minimal portal fibrosis were observed (grading 1 and staging 1, according to Ishak's scoring system) (Figure 1C,D). Confluent necrosis was not seen, nor was there a marked portal inflammatory infiltrate. Through the remaining 6 months, liver sections showed a stronger lobular and portal monuclear inflammation, with necroinflammatory activity ranging between mild and moderate grading. A mild-moderate pericellular fibrosis and intracytoplasmic cholestasis was also observed in several cases (Figure 1E,F). Lesions were not observed.

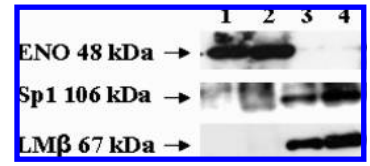

Figure 2. Check of fractions enrichment. WB analyses were performed to test cross-contamination of cytosolic (25 μg in lane 1 and 50 μg in lane 2) and nuclear (25 μg in lane 3 and 50 μg in lane 4) extracts from NTg liver. Enolase (ENO), Lamin β (LMβ) and Sp1 were used as markers of cytosolic fraction and nuclear fraction, respectively.

Table 1. Experimental Design of 2D-DIGE[a]

experiment	gel no.	Cy3	Cy5	Cy2
I	1	NTg	Tg	pooled standard
II	2	NTg	Tg	pooled standard
III	3	Tg	NTg	pooled standard

[a] Scheme of labeling used for both cytosolic and nuclear extracts.

Comparative Analysis of NTg and Tg Liver Proteomes by 2D-DIGE. We analyzed the changes in the hepatic proteome of NTg and Tg mice at early stages of LF (6 months). To increase the sensitivity of 2-D gels and the representation of low-abundance proteins, we analyzed the proteome in two different cellular fractions, enriched in either cytosolic or nuclear proteins. The qualitative enrichment of both cytosolic and nuclear fractions was checked by WB analyses using specific markers. Since cytosolic and nuclear fractions do not share housekeeping proteins to normalize the content of each marker, we loaded two different amounts of each fraction in order to better check the enrichment of each fraction. Enolase (ENO), the cytosolic marker, was exclusively detected in cytosolic fraction, while Lamin β (LMβ), a marker of structural component of the nuclear matrix, and the transcriptional factor Sp1, a marker of the soluble nuclear component, were exclusively detected in the nuclear fraction (Figure 2).

In this study, the differential protein expression profiles of cytosolic and nuclear extracts of 6-month-old Tg livers were compared, respectively, with those of NTg livers using DIGE in a pH nonlinear range 3.0−10.0 for cytosolic extracts, and 3.0−11.0 for nuclear extracts. Samples were labeled according to the scheme shown in Table 1. To increase the biological and statistical significance of results, we prepared both extracts from three different NTg and Tg livers. Accordingly, each experiment required two sets of gels (see Table 1). As summarized in Table 1, protein extracts were prelabeled with either Cy3 or Cy5 fluorescent dyes, and then each Cy3/Cy5-labeled sample pair was comixed with a Cy2-

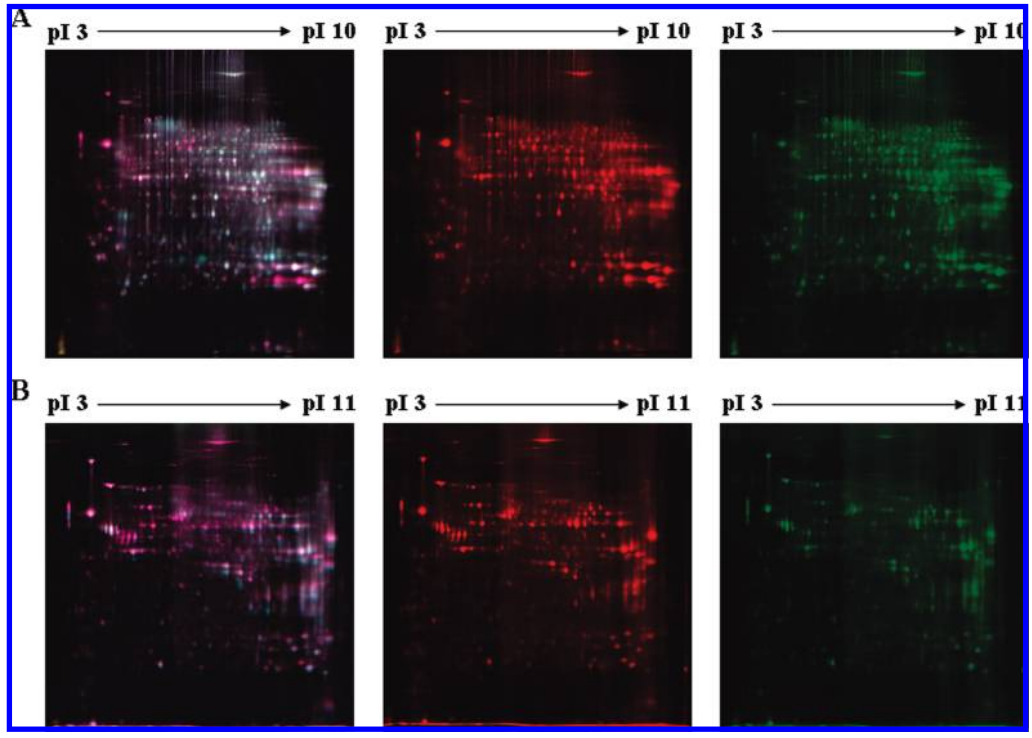

Figure 3. DIGE experiment. A representative picture of DIGE master gels images of both cytosolic (A) and nuclear (B) fractions of NTg and Tg livers is shown. For both A and B panels are shown: on the left, the overlay of three dye scan-images; on the center, the scan-image Cy5 of Tg liver; on the right, the scan-image Cy3 of NTg liver.

labeled pooled standard sample containing an equal amount of all six samples within the experiment both for cytosolic and nuclear fractions before running all three dye-labeled samples together on the same gel. Furthermore, in a third experiment, we interchanged Cy3 and Cy5 labeling design to avoid dye labeling-bias. For each gel, the Cy3, Cy5 and Cy2 images were imported into the DeCyder DIA (Difference In-gel Analysis) module to detect differentially expressed protein spot features in each gel. The Cy2 image increases the quality and reproducibility of 2-D gel analysis by allowing local spot normalization and by providing reference spots for further gel-to-gel matching. To identify the differentially expressed protein spots across the three gels, both for cytosolic and nuclear fractions, the results from the intragel comparison (three DIA files) were imported into the BVA (Biological Variation Analysis) module of DeCyder Software. For both cytosolic and nuclear fractions, one Cy2 image was selected as the master image, and the other two internal standard images were matched sequentially to it (Figure 3). For both extracts, the green spots in the overlay of three dye scan-images Cy2, Cy3 and Cy5 in Figure 3 represent the down-regulated spots, whereas the red spots represent the up-regulated spots in Tg liver. In Figure 3, the master gels DIGE images of both protein extracts of NTg (Cy3) and Tg (Cy5) livers are also shown. A total of ~3500 protein spots were identified on a typical cytosolic or nuclear liver extract gel using BVA software. We performed Student's paired *t* test ($p \leq 0.075$) to filter the protein spots that were differentially expressed between NTg and Tg livers. The statistical analysis identified in Tg liver 141 protein spots, representing statistically significant changes (fold change ≥ 1.75 or ≤ -1.75; p value ≤ 0.075) in cytosolic and nuclear proteins expression. In particular, 59 protein spots (28 up-regulated and 31 down-regulated) were from the cytosolic fraction, and 82 protein spots (66 up-regulated and 16 down-regulated) were from the nuclear fraction.

Identification of Differentially Expressed Proteins between NTg and Tg Livers and Validation. To identify differentially expressed proteins, 53 (25 cytosolic and 28 nuclear) spots of interest were excised from preparative gels, and in-gel trypsin digestion and MS analysis by MALDI were performed for protein identification. In this study, we were not able to pick-up the other differentially expressed spots from preparative gels in order to identify their protein components. This may in part be due to less sensibility and resolution power of Coomassie Colloidal Blue staining compared to fluorescence labeling, and insufficient amounts of protein in the spots. Successful identification was achieved if at least three peptides of experimental MALDI MS data with MS score ≥53 matched the internal sequence of the theoretical candidate protein. The MALDI MS analysis identified 38 (19 cytosolic and 19 nuclear) protein spots. The remaining (6 cytosolic and 9 nuclear) unidentified protein spots were further analyzed and identified by LC-MS MS analysis. The LC-MS MS analysis allows the identification of protein spots containing both low amounts of protein and complex peptide mixtures obtained from comigrated proteins. The results of protein identification are shown in Tables 2 and 3, and the positions of the differentially expressed spots picked-up in 2-D gels are shown in Figure 4. MS analysis identified 46 proteins, of which 6 [Actin, cytoplasmic 1 (ACTB); Aldehyde dehydrogenase, mitochondrial (ALDH2); Annexin A5 (ANXA5); Arginase-1 (ARG1); Glutamate dehydrogenase 1 (GLUD1); Glutathione *S*-transferase P1 (GSTP1)] were differentially expressed in both cytosolic and nuclear fractions. The presence of these proteins in both fractions could be explained considering that our protocol allowed the enrichment and not a complete purification of cytosolic or nuclear proteins in each fraction. In particular, 21 cytosolic and 19 nuclear protein spots

Table 2. Proteins Identified in the Cytosolic Fraction

LCMSMS	master number	protein name	protein symbol	ID NCBI	ID SPROT	MS score	MS match	theor. MW (Da)	experim. MW (Da)[a]	theor. p*I*	experim. p*I*[a]	Fold[b]	*P* value	subcellular location[c]
					Organic Acid Metabolism									
	2332	Arginase-1	ARG1	gi/71059675	Q61176	145	9	34927	40685	6.51	6.34	1.89	0.013	Cytoplasm
	1710	Glutamate dehydrogenase 1	GLUD1	gi/30931187	P26443	193	15	61640	52969	8.05	6.51	−3.69	0.0001	Mitochondrion matrix
	1715					205	18		52969		6.58	−4.85	8.60E-06	
*	2131	Long-chain specific acyl-CoA dehydrogenase, mitochondrial precursor	ACAD1	gi/12836858	P51174	481	14	48266	44470	8.34	6.31	−2.29	0.0002	Mitochondrion matrix
		Fumarylacetoacetase	FAH	gi/8569275	P35505	443	13	46704		6.99				NA
*	1787	Serine hydroxymethyltrasferase, cytosolic	SHMT1	gi/12845885	P50431	709	20	53168	51456	6.36	6.41	−3.08	0.066	Cytoplasm
*	2392	Fructose bisphosphatase 1	FBP1	gi/30411014	Q9QXD6	1043	19	37288	40000	6.15	6.04	−2.12	0.043	NA
					Alcohol Metabolism									
	1712	Aldehyde dehydrogenase 2, mitochondrial	ALDH2	gi/13529509	P47738	195	13	57015	52811	7.53	5.95	−2.47	0.033	Mitochondrion matrix
	1723					225	16		52600		6.1	−2.49	0.043	
*	3515	Hydroxymethylglutaryl-CoA synthase, mitochondrial precursor	HMGCS2	gi/555835	P54869	460	10	48384	23457	7.69	4.73	−2.05	0.02	Mitochondrion
	2500	Aldose 1-epimerase	GALM	gi/20381129	Q8K157	89	6	38003	38126	6.26	6.26	−1.95	0.034	Cytoplasm
					Glutathione Metabolism									
	3397	Glutathione S-transferase Theta-1	GSTT1	gi/1340076	Q64471	146	11	27643	25710	6.79	6.88	−2.77	0.0003	Cytoplasm
	3458	Glutathione S-transferase P1	GSTP1	gi/2624496	P19157	89	7	23521	24147	8.13	6.44	1.99	0.0018	NA
	3229	Glutathione S-transferase Mu 1	GSTM1	gi/28386202	P10649	215	16	26067	27885	7.71	6.72	−1.85	0.0096	Cytoplasm
	4673					230	17		26340		6.65	1.63	0.00029	
					Generation of Precursor Metabolites and Energy									
*	1852	Protein disulfide-isomerase A6 precursor	PDIA6	gi/74191305	Q922R8	604	11	49039	50136	5.04	5.08	2.81	0.0088	Endoplasmic reticulum lumen
		ATP synthase beta chain	ATP5B	gi/23272966	P56480	868	20	56632		5.24				Mitochondrion inner membrane
*	2131	Isovaleryl CoA dehydrogenase	IVD	gi/7689117	Q9JHI5	521	17	46695	44470	8.53	6.31	−2.29	0.0002	Mitochondrion matrix
	4652	Protein disulfide-isomerase precursor (PDI)	P4HB	gi/14250251	P09103	235	18	57422	55474	4.77	4.87	2.62	0.0033	Endoplasmic reticulum lumen
					Physiological Process									
*	820	Tumor rejection antigen	GRP94	gi/6755863	P08113	936	26	92703	75152	4.74	4.88	3.28	0.012	Endoplasmic reticulum lumen
	2898	3-Hydroxyanthranilate 3,4-dioxygenase (3-HAO)	HAAO	gi/15277547	Q78JT3	204	14	32955	32201	6.09	6.16	−2.03	0.02	Cytoplasm
	4670	Peroxiredoxin-1	PRDX1	gi/56103807	P35700	202	13	22390	24099	8.26	6.71	4.08	0.0033	Cytoplasm
*	3515	Tumour protein, translationally controlled 1 (TCTP)	TPT1	gi/55562869	P63028	128	3	19564	23457	4.76	4.73	−2.05	0.02	Cytoplasm
	3560	Gluthatione peroxidase 1	GPX1	gi/84871986	P11352	143	9	22544	22834	6.74	6.03	−1.8	0.0029	Cytoplasm
	2857	Annexin A5	ANXA5	gi/13277612	P48036	218	16	35773	32851	4.83	4.84	2.5	0.0021	NA
	2206	Actin, cytoplasmic 1	ACTB	gi/74213524	P60710	118	9	42066	43156	5.30	5.21	2.33	0.018	Cytoplasm, cytoskeleton
					Unknown Biologic'al Process[d]									
*	1787	Argininosuccinate lyase	ASL	gi/1674175	Q91YI0	690	20	51878	51456	6.48	6.41	−3.08	0.066	NA
	2654	Regucalcin	RGN	gi/15215231	Q64374	219	15	33899	35621	5.15	5.05	−3.63	0.051	Cytoplasm
	3268	Indolethylamine N-methyltrasferase	INMT	gi/15488762	P40936	69	4	30068	27387	6	5.66	−4.57	3.00E-05	Cytoplasm
	4676					128	9		27387		5.89	−4.6	1.70E-06	

[a] Experimental MW and p*I* were calculated by DeCyder 5.0 software. [b] Fold is the ratio between the protein expression level of Tg and the protein expression level of NTg (Tg/NTg). [c] Searching for subcellular location was performed on Swiss-Prot database. NA: not available. [d] These proteins were not associated with any biological process. They were classified in molecular functional category as calcium ion binding (Q91Y10, Q64374) and *S*-methyltransferase activity (P40936).

Table 3. Proteins Identified in the Nuclear Fraction

LCMSMS	master number	protein name	protein symbol	ID NCBI	ID SPROT	MS score	MS match	theor. MW (Da)	experim. MW (Da)[a]	theor. p*I*	experim. p*I*[a]	fold[b]	*P* value	subcellular location[c]
						Cofactor Metabolism								
	805	Aconitase 2, mitochondrial	ACO2	gi/63101587	Q99KI0	130	12	86185	67618	8.08	7.33	2.23	0.0029	Mitochondrion
	810					154	15		67502		7.57	2.21	2.2E-05	
*	1649	Dihydrolipoamide S-succinyltransferase	DLST	gi/21313536	Q9D2G2	140	2	49306	51417	9.11	6.24	2.67	7.2E-05	Mitochondrion
*	3573	ATP synthase D chain, mitochondrial	ATP5H	gi/51980458	Q9DCX2	226	4	18795	25594	5.52	5.13	−2.13	0.00037	Mitochondrion inner membrane
		Heme-binding protein 1	HEBP1	gi/71059853	Q9R257	185	8	21153		5.18				Cytoplasm
*	1585	ATP synthase alpha chain	ATP5A1	gi/6680748	Q03265	725	12	59830	52981	9.22	7.56	−1.98	0.041	Mitochondrion inner membrane
*	1962	GTP-specific succinyl Co-A	SUCLG2	gi/3766203	Q9Z2I8	274	7	44115	45105	5.91	5.66	1.86	0.001	Mitochondrion
	3078	Glutathione S-transferase P1	GSTP1	gi/2624496	P19157	115	9	23521	25179	8.13	7.83	4.97	0.0074	NA
						Cellular Catabolism								
*	3008	Arginase-1	ARG1	gi/74146247	Q61176	158	3	36423	25925	6.33	6.2	3.01	0.0011	Cytoplasm
	2221					204	14		40459		6.55	−2.18	0.0096	
	2225					213	16		40286		6.74	−2.84	0.0021	
*	1585	Catalase	CAT	gi/26344712	P24270	257	6	59882	52981	7.72	7.56	−1.98	0.041	Peroxisome
	1897	Ornithine aminotransferase	OAT	gi/14198116	P29758	225	19	48723	47470	6.19	5.88	3.05	0.016	Mitochondrion matrix
						Metabolism								
*	1800	Ubiquinol-cytochrome-c reductase	UQCRC1	gi/12850298	Q9CZ13	612	12	53420	48759	5.75	5.39	2	0.0058	Mitochondrion inner membrane
*	1383	T-complex protein 1 subunit theta	CCT8	gi/12846632	P42932	381	10	59957	57126	5.44	5.75	2.51	0.00028	Cytoplasm
*	3573	Glyoxalase 1	GLO1	gi/19354350	Q9CPU0	218	5	20997	25594	5.24	5.13	−2.13	0.00037	NA
*	1585	Glutamate dehydrogenase 1	GLUD1	gi/30931187	P26443	464	12	61640	52981	8.05	7.56	−1.98	0.041	Mitochondrion matrix
*	3008	High mobility group 1 protein	HMGB1	gi/600761	P63158	102	5	25019	25925	5.75	6.2	3.01	0.0011	Nucleus
*	3559					149	4		26192		6.37	−2.21	0.001	
*	1532	Aldehyde dehydrogenase 2, mitochondrial	ALDH2	gi/6753036	P47738	294	7	57015	54219	7.53	5.89	2.6	0.0001	Mitochondrion matrix
*	1649					293	6		51417		6.24	2.67	7.2E-05	
	1668					205	13		51241		6.42	2.86	2.4E-05	
						Physiological Process								
*	1800	Actin, cytoplasmic 1	ACTB	gi/74178273	P60710	392	12	42052	48759	5.29	5.39	2	0.0058	Cytoplasm, cytoskeleton
*	1962					274	8		45105		5.66	1.86	0.001	
	1961	Actin, cytoplasmic 2	ACTG1	gi/54696574	P63260	136	13	42108	45183	5.31	5.48	1.88	0.0081	Cytoplasm, cytoskeleton
						Response to Stress								
	2547	Annexin A5	ANXA5	gi/1098603	P48036	135	9	35787	33413	4.83	4.91	2.63	5.2E-05	NA
*	1383	60 KDa heat shock protein	HSPD1	gi/76779273	P63038	746	20	61088	57126	5.91	5.75	2.51	0.00028	Mitochondrion matrix
	1394					184	17		57028		5.48	2.47	9.9E-05	
	1404					202	17		56882		5.61	2.86	1.4E-05	
*	1532					149	4		54219		5.89	2.6	0.0001	
*	1962	78 kDa glucose regulated protein precursor	GRP78	gi/2598562	P20029	493	10	72492	45105	5.07	5.66	1.86	0.001	Endoplasmic reticulum lumen
*	1383	Heat shock protein 9A	HSPA9A	gi/6754256	P38647	202	4	73768	57126	5.91	5.75	2.51	0.00028	Mitochondrion
*	1532	Keratin, type II cytoskeletal 8	KRT8	gi/76779293	P11679	563	11	54400	54219	5.7	5.89	2.6	0.0001	NA
	1548					196	16		53803		5.81	2.82	0.0016	
	1552					229	20		53757		5.95	2.44	0.0015	
	1557					279	26		53619		6.07	2.73	2.2E-07	
	1658					328	25		51637		5.65	3.21	0.0015	
	1627					211	15		51859		5.48	2.94	0.026	
	1633					301	23		51770		5.82	3.05	0.0038	
	3525					187	22		54452		6.00	2.17	8.9E-06	
*	1800	Keratin, type I cytoskeletal 18	KRT18	gi/74198485	P05784	1143	21	47437	48759	5.27	5.39	2	0.0058	NA
	1811					273	20		48676		5.3	4.57	0.0047	
						Unknown Biological Process[d]								
*	1649	Heterogeneous nuclear ribonucleoprotein H′	HNRPH2	gi/13529467	P70333	179	5	49533	51417	5.89	6.24	2.67	7.2E-05	Nucleus, nucleoplasm
*	3559	Chain L, polysaccaride binding antibody	2H1P_L	gi/2914304		143	4	24370	26192	6.57	6.37	−2.21	0.001	NA

[a] Experimental MW and p*I* were calculated by DeCyder 5.0 software. [b] Fold is the ratio between the protein expression level of Tg and the protein expression level of NTg (Tg/NTg). [c] Searching for subcellular location was performed on Swiss-Prot database. NA: not available. [d] These proteins were not associated with any biological process. P70333 was classified in molecular functional category as nucleic acid binding.

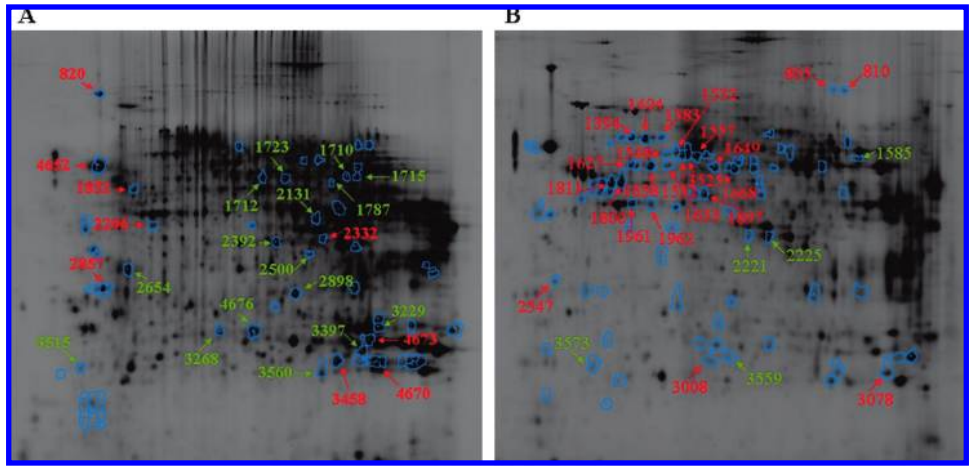

Figure 4. Maps of 2-D gels. The differentially expressed cytosolic (A) and nuclear (B) spots between NTg and Tg livers are shown. The arrows show picked-up and identified spots. The red spots were up-regulated, while the green spots were down-regulated in Tg liver.

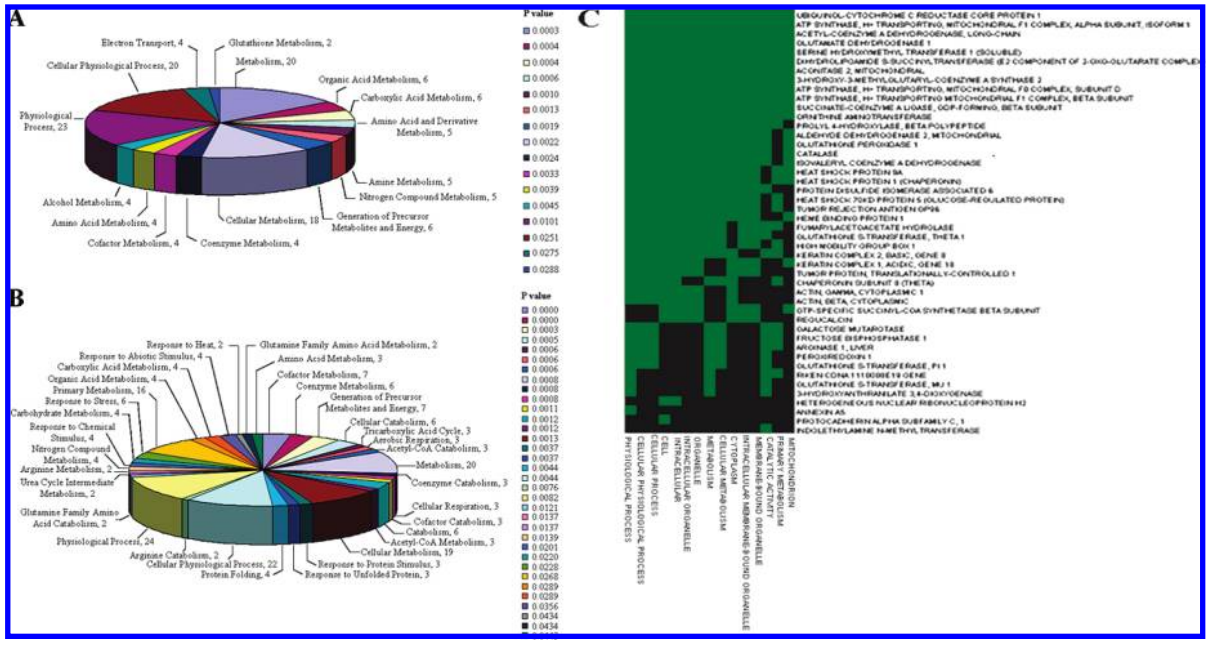

Figure 5. Data mining of identified proteins. Identified proteins were classified using DAVID 2.1 beta annotation system. A and B graphics show cytosolic and nuclear proteins ontology analyses, respectively. The Fisher exact test was used to determine the protein-enrichment in annotation terms. The numbers near functional categories terms, sorted by *p*-value, indicate the number of proteins within each functional category. (C) Shows Functional Annotation Clustering analysis performed on total identified proteins. The identified proteins are shown in the different lines, the functional categories are shown in the columns. The green squares indicate the corresponding protein-term association positively reported.

were identified as a unique protein, while the remaining (4 cytosolic and 9 nuclear) protein spots contained more than one protein, indicating some different proteins comigrated in the same spot under our experimental condition. In several cases, some well-separated spots of similar mass but different p*I* were identified as the same protein. This could be the result of alternative post-translational modifications, such as phosphorylation or deamidation, or multiple expression forms. These possibilities have not been studied further to date. Moreover, 78 kDa glucose regulated protein (GRP78; nuclear spot no. 1962) and Arginase-1 (ARG1; nuclear spot no. 3008) were detected in spots which differed from their theoretical molecular weight, and Hydroxymethylglutaryl-CoA synthase (HMGCS2; cytosolic spot no. 3515) was detected in a spot which differed from its theoretical molecular weight and p*I*. These could reflect proteolytic degradation of these proteins or post-translational modifications, such as glycosylation.

We performed functional classification of identified proteins according to DAVID 2.1 beta annotation system. The ontology analysis of identified cytosolic proteins (Figure 5A) indicated the most statistically relevant functional categories were Metabolism, Organic Acid Metabolism, and Carboxylic Acid Metabolism. Cofactor metabolism and Coenzyme Metabolism were the most statistically relevant functional categories in the list of identified proteins from nuclei-enriched fraction (Figure 5B). Furthermore, the functional categories containing proteins involved in stress response (Response to Protein Stimulus, Response to Heat, Response to Abiotic Stimulus, Response to Unfolded Protein, Protein Folding, Response to Stress, and Response to Chemical Stimulus) were also present in the list of identified proteins from

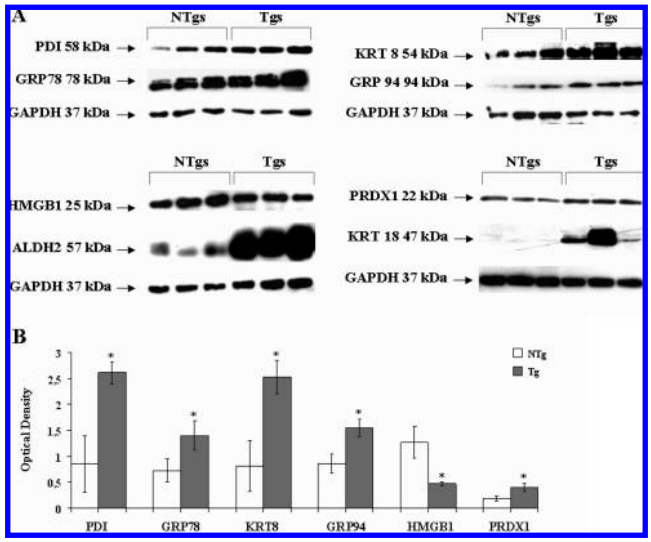

Figure 6. Validation of DIGE data. (A) WB analyses of selected proteins were performed on total protein extracts of 6-month-old NTg and Tg livers. The extracts were prepared from three different NTg and Tg livers. GAPDH was used as loading control. (B) The densitometer analyses were performed only for the proteins which did not show abundant variation of expression (PDI, GRP78, KRT8, GRP94, HMGB1, and PRDX1). The signal intensity of specific bands was determined by a densitometer. The levels of each protein in each sample were normalized to those of GAPDH. The *y*-axis shows the optical density of protein expression. The data were presented as average and standard deviation. * Student's *t* test; *p*-value ≤ 0.05.

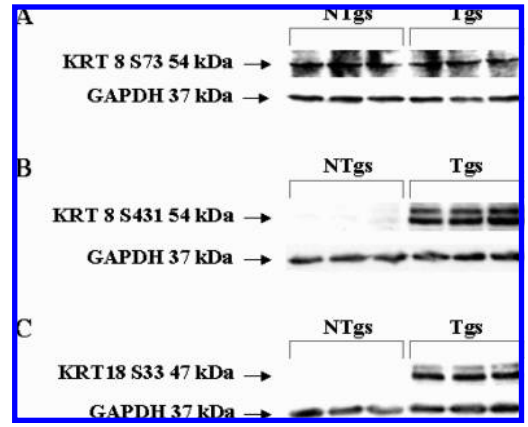

Figure 7. Keratin phosphorylation in Tg and NTg livers. WB analyses of KRT8 phospho S73 (A), KRT8 phospho S431 (B), and KRT18 phospho S33 (C) proteins were performed on total protein extracts of 6-month-old NTg and Tg livers. The extracts were prepared from three different NTg and Tg livers. GAPDH was used as loading control.

nuclei-enriched fraction (Figure 5B). Functional Annotation Clustering analysis, performed on total identified proteins, showed a group of terms having similar biological meaning due to sharing similar protein members. The green color corresponds to the protein-term association positively reported, while the black color corresponds to the protein-term association not reported yet. The proteins at the top of graphic in plenty green area explain much better the biology of the disease because of the more common functional annotations (Figure 5C).

We validated the differential expression of some identified proteins [Protein disulfide-isomerase (PDI); 78 kDa glucose regulated protein (GRP78), High mobility group 1 protein (HMGB1), Aldehyde dehydrogenase 2, mitochondrial (ALDH2), Keratin, type II cytoskeletal 8 (KRT8), Keratin, type 1 cytoskeletal 18 (KRT18), Tumor rejection antigen (GRP94), Peroxiredoxin-1 (PRDX1)] based on the availability of good commercial antibodies by WB analyses. To increase the biological significance of the results, we performed WB analyses on total extracts of three NTg and Tg livers that were different from those used for DIGE experiments (Figure 6A). GAPDH was used as loading control of each sample. Semiquantitative analyses of protein expression were performed only for PDI, GRP78, KRT8, GRP94, HMGB1, and PRDX1 which did not show abundant variation of expression (Figure 6B). WB results showed significant PDI, GRP78, ALDH2, KRT8, KRT18, GRP94, and PRDX1 protein up-regulation in Tg livers' total extracts compared to NTg livers' total extracts. Moreover, WB results showed significant HMGB1 protein down-regulation in Tg livers' total extracts compared to those of NTg livers. HMGB1 protein was detected in two different protein spots from nuclei-enriched fraction (3008 and 3559) that showed similar molecular weight, but different p*I* and regulation (3008 spot was up-regulated, while 3559 spot was down-regulated). MS analysis performed on these protein spots identified comigrated proteins; in fact, 3008 spot contained ARG1 and HMGB1, while 3559 spot contained Chain L, polysaccaride binding antibody (2H1P_L) and HMGB1. Together these data indicate that HMGB1 protein was down-regulated in Tg livers' total extracts, and its different regulation probably is the result of comigrated proteins regulation and/or of alternative post-translational modifications, such as phosphorylation. These possibilities have not been studied further to date.

Keratin Phosphorylation in Tg and NTg Livers. In Tg liver, we observed increased expression of KRT8 and KRT18 (Figure 6). In addition, in the 2D-DIGE experiment, these proteins were identified in several well-separated spots of similar mass but different p*I*, indicating they could have undergone post-translational modifications. To analyze the phosphorylation status of KRT8 and KRT18 in NTg and Tg livers, we performed WB analyses on total protein extracts of three NTg and Tg livers that were different from those used for DIGE experiments (Figure 7). GAPDH was used as loading control of each sample. As shown in Figure 7, KRT8 was phosphorylated on serine 431 in Tg compared to NTg samples, while the phosphorylation of KRT8 on serine 73 did not change between the Tg and NTg samples. Moreover, phosphorylation of KRT18 on serine 33 in Tg samples was also observed.

Superoxide Dismutase (SOD) Expression in Tg and NTg Livers. To analyze the expression of SOD in NTg and Tg livers, we performed WB analysis on total protein extracts of three NTg and Tg livers that were different from those used for DIGE experiments. GAPDH was used as loading control of each sample. WB results showed SOD expression did not change between NTg and Tg livers (data not shown).

Discussion

Liver diseases afflict more than 10% of the world's population; however, strategies for their diagnosis, staging, and treatment remain limited. Fibrosis and its consequence, cirrhosis, represent long-term processes which are associated with major modifications of ECM proteins. Before fibrosis and cirrhosis can be easily observed at the histological level, many changes in the protein expression profile of hepatic fibroblasts are thought to occur. Since the potential of proteomics in discovery-based research is tremendous, proteomic technolo-

gies can be used to identify protein markers and/or signatures for the early detection of fibrosis-associated events. Until now, proteomic technologies have been used to analyze serum from HBV and hepatitis C virus infected patients, to unravel serum protein signatures to help differentiate between different stages of fibrosis and predict fibrosis and cirrhosis in chronic hepatitis B and C infection,[23,24] identify serum biomarkers for early detection of liver cirrhosis using rat models,[25] and to analyze the total liver proteome of fibrosis and cirrhosis animal models.[26–28] These studies performed on animal models have allowed us to increase our understanding of LF pathogenesis. In fact, they describe a potentially dynamic process, and the serial sampling of tissue in the volume required for detailed studies of cellular and molecular pathogenesis. Additionally, the development of modern molecular tools and genetically modified mice suggests that mouse models can be applied to LF mechanistic studies in which individual mediators or cell types are deregulated. Therefore, to understand the LF molecular mechanisms, animal models are more useful than cell culture models (which cannot recapitulate the events that occur in vivo resulting from the complex interplay of resident and incoming cells in a microenvironment) and human tissues taken at biopsy or following hepatic resection (for which ethical considerations prevent multiple liver biopsies being taken from patients for research purposes and data generated tends to be representative only of relatively advanced disease).

To our knowledge, this study is the first proteomic investigation performed on an animal model of hepatitis B infection induced fibrosis. The histopathological characterization of Tg used in this study demonstrated the onset of fibrosis at 6 months and the progressive fibrosis development through the remaining 6 months. In this paper, our attention was focused on early stages of LF. However, this animal model potentially could also allow the study of the dynamic process of hepatic fibrogenesis by analyzing Tg liver proteome at 9 and 12 months of life.

The main aim of our study was to perform, using 2-D DIGE technology, a comparative analysis of cytosolic and nuclear protein expression patterns found in Tg and NTg livers at the early stages of LF in order to discover new putative protein markers to be used in early detection of LF. On the basis of previously published studies in which the hepatic proteome changes of LF induced animal models were analyzed in total liver extracts, we analyzed the hepatic proteome changes of Tg at the early stages of LF in two subcellular fractions enriched in either cytosolic or nuclear proteins in order to improve low-abundance protein detection and 2-D electrophoresis resolution. We detected a total of 59 protein spots in the cytosolic fraction and 82 protein spots in the nuclear fraction that showed differences in their relative expression between NTg and Tg livers. Fifty-three protein spots were picked-up and 46 proteins were identified. Closed examination of the identified differentially expressed proteins showed that those of greatest relevance are annotated to the Organic Acid Metabolism and Cofactor Metabolism functional categories. Most of the proteins related to Organic Acid Metabolism were down-regulated, while most of the proteins related to Cofactor Metabolism were up-regulated at early stages of LF.

Changes in protein expression included the up-regulation of proteins involved in stress response. These changes were consistent with the biological process in study and occurred early. Mammalian cells express a family of highly conserved proteins in response to heat as well as many other stressful stimuli.[29] This family of stress proteins includes heat shock proteins (HSPs) and glucose regulated proteins (GRPs).[30,31] These proteins are multifunctional molecular chaperones that participate in the complex formation of many proteins, contribute to the folding and extension of proteins as well as the assembly of polycomplex, function in protein transport between cell organelles, and regulate target proteins other than changes of their construction. Remarkable was the increased expression of GRP94, which activates both innate and adaptive immunity[32,33] and plays a role in hepatocarcinogenesis,[34] and GRP78, which may play a role in facilitating the assembly of multimeric protein complexes inside endoplasmic reticulum. Recently, it has been demonstrated that GRP94 expression increased as HBV-induced disease progressed from chronic hepatitis to cirrhosis and then to HCC.[35,36] Furthermore, previous data showed that the expression of GRP78, GRP94, HSP90, or HSP70 stress proteins is closely correlated with tumor progression and HBV-related HCC aggressive behavior. In particular, it was suggested that GRP78 and GRP94 might play a role in early stage HBV-related hepatocarcinogenesis, and GRP78, GRP94, and HSP90 may be important prognostic markers which strongly suggest the presence of vascular invasion and intrahepatic metastasis.[34] GRP78 and GRP94 increased expression during early stages of LF in Tg livers emphasizes the role played by these proteins in HBV-induced development of liver disease and suggests these proteins might be valuable diagnostic or prognostic markers of HBV-induced liver disease progression both for early (fibrosis/cirrhosis) and late (HCC) stages. Further work needs to be performed to elucidate a conclusive implication.

KRT8 and KRT18 play an important role in protecting the liver from mechanical and nonmechanical forms of stress. In Tg liver, we observed increased expression of KRT8 and KRT18 (Figure 6), and the phosphorylation of KRT8 on serine 431 and KRT18 on serine 33 (Figure 7). In addition, differential expression of the KRT18 gene in the fibrotic area of Tg liver was further demonstrated by Quantitative Real Time PCR experiments performed on RNA extracted from cell elements involved in LF excised using laser capture microdissection technology (Materials and Methods, Results, and Figure 1S in Supporting Information). KRT8 and KRT18 hyperphosphorylation is a liver disease progression marker in hepatitis C affected patients.[37] Moreover, KRT8 and KRT18 variants were detected in hepatitis C affected patients and their presence correlated with fibrosis progression.[38] Therefore, increased expression of KRT8 and KRT18 phosphorilated variants in Tg liver opens the possibility to use KRT8 and KRT18 hyperphosphorylation as a marker of liver disease progression in HBV infected patients too. The potential use of keratin phosphorylation as a diagnostic marker will need to await additional confirmatory studies. Potential applications include assessment of keratin phosphorylation in liver biopsies, or possibly screening serum for the presence of phosphokeratin protein or peptide fragments leaked from damaged hepatocytes, or for the presence of autophosphokeratin antibodies.

A free radical metabolism deregulation in Tg liver is suggested by decreased expression of two critical enzymes of the antioxidant defense system: Glutathione peroxidise 1 (GPX1) and Catalase (CAT). WB analysis performed on total protein extracts of NTg and Tg livers did not show the down-regulation of another important enzyme of this system (data not shown): Superoxide Dismutase. However, GPX1 and CAT down-regulated expression could determine an increase of oxidative damage in Tg liver.

We also observed ALDH2 up-regulation in fibrotic liver samples (Figure 6). This up-regulation is a strong indication for the presence of increased lipid peroxides and indicates oxidative stress in Tg liver. The up-regulation of KRT8, KRT18,

ACTB and Actin cytoplasmic 2 (ACTG1) structural proteins was also observed in Tg liver in agreement with the biological process in study and occurred early. Of interest was also the decreased expression of HMGB1 protein (Figure 6). This protein plays a role in contributing to virus-specific cytotoxic T lymphocytes induced liver disease in Tg livers, and HMGB1 inhibitors decrease the severity of hepatitis in this animal model.[40] Therefore, the inhibitors that target HMGB1 may be useful for treatment of chronically HBV-infected patients.

Glutathione-*S*-transferases (GSTs) are a family of phase II detoxification enzymes that play an important role in protecting cells from cytotoxic and carcinogenic agents by catalyzing the conjugation of many hydrophobic and electrophilic compounds with reduced glutathione,[41] resulting in less toxic and more readily excreted metabolites. These enzymes may help defend hepatocytes against a variety of potentially promutagenic stresses, including reactive oxygen species associated with chronic hepatic inflammation and reactive electrophilic compounds associated with the hepatic metabolism of dietary carcinogens.[42–46] The importance of the role played by GST in HBV-related liver disease development is emphasized by the significant association between GSTP1 and GSTM1 gene polymorphisms and development of HBV-related chronic liver disease[47] and by the association of particular GST alleles with altered risk or outcome of HBV-related HCC.[48]

Conclusion

In this work, we have used 2D-DIGE technique to analyze the proteome of Tg liver at early stages of fibrosis. We identified at least 53 protein spots corresponding to 46 proteins that were differentially expressed in fibrotic liver, and that have important roles in a variety of pathways. In addition to a number of proteins which have been already found differentially expressed in animal models of liver injury (ARG1, GRP94, GPR78, PDIA6, ALDH2, HMGCS2, ACAD1, CAT, GPX1, RGN, GSTP1, ACO2, HAAO, PRDX1, GLUD1 and IVD),[26,27,49,50] and related to liver injury in humans (GSTM1, GSTT1, GSTP1, ALDH2, ASL, FAH, FBP1, RGN, GPX1, CAT, GLO1, KRT8 and KRT18),[37,38,51–63] these proteins and newly identified ones were related to hepatitis B infection induced fibrosis.

These results strengthen the use of proteomic technologies applied to the Tg model to discover new putative biomarkers and/or protein expression signature for early detection of LF. Further studies performed on selected population of HBV infected patients will be necessary to confirm the data obtained using this hepatitis B-infected mouse model in order to identify biochemical markers for diagnosis and prognosis of HBV induced fibrosis, targets for therapy and treatment of HBV induced fibrosis.

Acknowledgment. We thank Prof. Piero Pucci and his collaborators for MS identifications, Dr. Silvia Esposito for technical assistance, Prof. Giancarlo Troncone and his collaborators for LCM facility, Centro Regionale di Competenza GEAR, regione Campania, for 2D-DIGE facility, the financial support of grants Convenzione CEINGE-Regione Campania-Ass. Sanità, and the financial support of Associazione Italiana per la Ricerca sul Cancro AIRC. The salary of Dr. Daniela Spano was supported by Ministero dell'Università e della Ricerca Italiano, grants for MUR-P35/126/IND. The salary of Dr. Flora Cimmino was supported by Fondazione per la lotta al Neuroblastoma-ONLUS. Dr. Mario Capasso is a fellow of Fondazione Italiana per la Ricerca sul Cancro, FIRC.

Supporting Information Available: Materials and Methods, Results, and Supplementary Figure 1 (Figure 1S)" on the analysis of KRT18 gene expression in fibrotic area of Tg liver by laser capture microdissection (LCM). This material is available free of charge via the Internet at http://pubs.acs.org.

References

(1) Friedman, S. L. Liver fibrosis sbdfrom bench to bedside. *J. Hepatol.* **2003**, *38* (Suppl. 1), S38–S53.
(2) Poynard, T.; Ratziu, V.; Benhamou, Y.; Opolon, P.; Cacoub, P.; Bedossa, P. Natural history of HCV infection. *Baillieres Best Pract. Res. Clin. Gastroenterol.* **2000**, *14* (2), 211–228.
(3) Gines, P.; Cardenas, A.; Arroyo, V.; Rodes, J. Management of cirrhosis and ascites. *N. Engl. J. Med.* **2004**, *350*, 1646–1654.
(4) McKillop, I. H.; Moran, D. M.; Jin, X.; Koniaris, L. G. Molecular pathogenesis of hepatocellular carcinoma. *J. Surg. Res.* **2006**, *136* (1), 125–135.
(5) Higuchi, H.; Gores, G. J. Mechanisms of liver injury: an overview. *Curr. Mol. Med.* **2003**, *3* (6), 483–490.
(6) Iredale, J. P. Cirrhosis: new research provides a basis for rational and targeted treatments. *Br. Med. J.* **2003**, *327*, 143–147.
(7) Afdhal, N. H.; Nunes, D. Evaluation of liver fibrosis: a concise review. *Am. J. Gastroenterol.* **2004**, *99* (6), 1160–1174.
(8) Thampanitchawong, P.; Piratvisuth, T. Liver biopsy: complications and risk factors. *World J. Gastroenterol.* **1999**, *5* (4), 301–304.
(9) Regev, A.; Berho, M.; Jeffers, L. J.; Milikowski, C.; Molina, E. G.; Pyrsopoulos, N. T.; Feng, Z. Z.; Reddy, K. R.; Schiff, E. R. Sampling error and intra-observer variation in liver biopsy in patients with chronic HCV infection. *Am. J. Gastroenterol.* **2002**, *97* (10), 2614–2618.
(10) Tonge, R.; Shaw, J.; Middleton, B.; Rowlinson, R.; Rayner, S.; Young, J.; Pognan, F.; Hawkins, E.; Currie, I.; Davison, M. Validation and development of fluorescence two-dimensional differential gel electrophoresis proteomics technology. *Proteomics* **2001**, *1* (3), 377–396.
(11) Chisari, F. V.; Klopchin, K.; Moriyama, T.; Pasquinelli, C.; Dunsford, H. A.; Sell, S.; Pinkert, C. A.; Brinster, R. L.; Palmiter, R. D. Molecular pathogenesis of hepatocellular carcinoma in hepatitis B virus transgenic mice. *Cell* **1989**, *59* (6), 1145–1156.
(12) Constandinou, C.; Henderson, N.; Iredale, J. P. Modelling liver fibrosis in rodents. *Methods Mol. Med.* **2005**, *117*, 237–250.
(13) Tsukamoto, H.; Matsuoka, M.; French, S. W. Experimental models of hepatic fibrosis: a review. *Semin. Liver Dis.* **1990**, *10*, 56–65.
(14) Chisari, F. V.; Pinkert, C. A.; Milich, D. R.; Filippi, P.; McLachlan, A.; Palmiter, R. D.; Brinster, R. L. A transgenic mouse model of the chronic hepatitis B surface antigen carrier state. *Science* **1985**, *230* (4730), 1157–1160.
(15) Chisari, F. V.; Filippi, P.; Buras, J.; McLachlan, A.; Popper, H.; Pinkert, C. A.; Palmiter, R. D.; Brinster, R. L. Structural and pathological effects of synthesis of hepatitis B virus large envelope polypeptide in transgenic mice. *Proc. Natl. Acad. Sci. U.S.A.* **1987**, *84*, 6909–6913.
(16) Dunsford, H. A.; Sell, S.; Chisari, F. V. Hepatocarcinogenesis due to chronic liver cell injury in hepatitis B virus transgenic mice. *Cancer Res.* **1990**, *50*, 3400–3407.
(17) Toshkov, I.; Chisari, F. V.; Bannasch, P. Hepatic preneoplasia in hepatitis virus transgenic mice. *Hepatology* **1994**, *20*, 1162–1172.
(18) Huang, S. N.; Chisari, F. V. Strong, sustained hepatocellular proliferation precedes hepatocarcinogenesis in hepatitis B surface antigen transgenic mice. *Hepatology* **1995**, *21*, 620–626.
(19) Dathan, N.; Parlato, R.; Rosica, A.; De Felice, M.; Di Lauro, R. Distribution of the titf2/foxe1 gene product is consistent with an important role in the development of foregut endoderm, palate, and hair. *Dev. Dyn.* **2002**, *224* (4), 450–456.
(20) Ishak, K.; Baptista, A.; Bianchi, L.; Callea, F.; De Groote, J.; Gudat, F.; Denk, H.; Desmet, V.; Korb, G.; MacSween, R. N.; et al. Histological grading and staging of chronic hepatitis. *J. Hepatol.* **1995**, *22* (6), 696–699.
(21) Cimmino, F.; Spano, D.; Capasso, M.; Zambrano, N.; Russo, R.; Zollo, M.; Iolascon, A. Comparative Proteomic Expression Profile in All-trans Retinoic Acid Differentiated Neuroblastoma Cell Line. *J. Proteome Res.* **2007**, *6* (7), 2550–2564.
(22) Dennis, G., Jr.; Sherman, B. T.; Hosack, D. A.; Yang, J.; Gao, W.; Lane, H. C.; Lempicki, R. A. DAVID: Database for Annotation, Visualization, and Integrated Discovery. *GenomeBiology* **2003**, *4* (5), P3.
(23) Poon, T. C.; Hui, A. Y.; Chan, H. L.; Ang, I. L.; Chow, S. M.; Wong, N.; Sung, J. J. Prediction of liver fibrosis and cirrhosis in chronic

hepatitis B infection by serum proteomic fingerprinting: a pilot study. *Clin. Chem.* **2005**, *51* (2), 328–335.
(24) Göbel, T.; Vorderwülbecke, S.; Hauck, K.; Fey, H.; Häussinger, D.; Erhardt, A. New multi protein patterns differentiate liver fibrosis stages and hepatocellular carcinoma in chronic hepatitis C serum samples. *World J. Gastroenterol.* **2006**, *12* (47), 7604–7612.
(25) Xu, X. Q.; Leow, C. K.; Lu, X.; Zhang, X.;.; Liu, J. S.; Wong, W. H.; Asperger, A.; Deininger, S.; Eastwood Leung, H. C. Molecular classification of liver cirrhosis in a rat model by proteomics and bioinformatics. *Proteomics* **2004**, *4* (10), 3235–3245.
(26) Low, T. Y.; Leow, C. K.; Salto-Tellez, M.; Chung, M. C. A proteomic analysis of thioacetamide-induced hepatotoxicity and cirrhosis in rat livers. *Proteomics* **2004**, *4* (12), 3960–3974.
(27) Henkel, C.; Roderfeld, M.; Weiskirchen, R.; Berres, M. L.; Hillebrandt, S.; Lammert, F.; Meyer, H. E.; Stühler, K.; Graf, J.; Roeb, E. Changes of the hepatic proteome in murine models for toxically induced fibrogenesis and sclerosing cholangitis. *Proteomics* **2006**, *6* (24), 6538–6548.
(28) Do, S. H.; Yun, H. S.; Jeong, W. I.; Jeong, D. H.; Ki, M. R.; Chung, J. Y.; Park, S. J.; Kim, S. B.; Jeong, K. S. Up-regulation of Metabotropic glutamate receptor 3 (mGluR3) in rat fibrosis and cirrhosis model of persistent hypoxic condition. *Mol. Cell. Biochem.* **2007**, *294* (1−2), 189–196.
(29) Lindquist, S.; Craig, E. A. The heat-shock proteins. *Annu. Rev. Genet.* **1988**, *22*, 631–677.
(30) Little, E.; Ramakrishnan, M.; Roy, B.; Gazit, G.; Lee, A. S. The glucose-regulated proteins (GRP78 and GRP94): functions, gene regulation, and applications. *Crit. Rev. Eukaryotic Gene Expression* **1994**, *4*, 1–18.
(31) Garrido, C.; Gurbuxani, S.; Ravagnan, L.; Kroemer, G. Heat shock proteins: endogenous modulators of apoptotic cell death. *Biochem. Biophys. Res. Commun.* **2001**, *286*, 433–442.
(32) Srivastava, P. Roles of heat-shock proteins in innate and adaptive immunity. *Nat. Rev. Immunol.* **2002**, *2*, 185–194.
(33) Srivastava, P. Interaction of heat shock proteins with peptides and antigen presenting cells: chaperoning of the innate and adaptive immune responses. *Annu. Rev. Immunol.* **2002**, *20*, 395–425.
(34) Lim, S. O.; Park, S. G.; Yoo, J. H.; Park, Y. M.; Kim, H. J.; Jang, K. T.; Cho, J. W.; Yoo, B. C.; Jung, G. H.; Park, C. K. Expression of heat shock proteins (HSP27, HSP60, HSP70, HSP90, GRP78, GRP94) in hepatitis B virus-related hepatocellular carcinomas and dysplastic nodules. *World J. Gastroenterol.* **2005**, *11* (14), 2072–2079.
(35) Zhu, X. D.; Li, C. L.; Lang, Z. W.; Gao, G. F.; Tien, P. Significant correlation between expression level of HSP gp96 and progression of hepatitis B virus induced diseases. *World J. Gastroenterol.* **2004**, *10* (8), 1141–1145.
(36) Yao, D. F.; Wu, X. H.; Su, X. Q.; Yao, M.; Wu, W.; Qiu, L. W.; Zou, L.; Meng, X. Y. Abnormal expression of HSP gp96 associated with HBV replication in human hepatocellular carcinoma. *Hepatobiliary Pancreat. Dis. Int.* **2006**, *5* (3), 381–386.
(37) Toivola, D. M.; Ku, N. O.; Resurreccion, E. Z.; Nelson, D. R.; Wright, T. L.; Omary, M. B. Keratin 8 and 18 hyperphosphorylation is a marker of progression of human liver disease. *Hepatology* **2004**, *40* (2), 459–466.
(38) Strnad, P.; Lienau, T. C.; Tao, G. Z.; Lazzeroni, L. C.; Stickel, F.; Schuppan, D.; Omary, M. B. Keratin variants associate with progression of fibrosis during chronic hepatitis C infection. *Hepatology* **2006**, *43* (6), 1354–1363.
(39) Fukaya, Y.; Yamaguchi, M. Regucalcin increases superoxide dismutase activity in rat liver cytosol. *Biol. Pharm. Bull.* **2004**, *27* (9), 1444–1446.
(40) Sitia, G.; Iannacone, M.; Müller, S.; Bianchi, M. E.; Guidotti, L. G. Treatment with HMGB1 inhibitors diminishes CTL-induced liver disease in HBV transgenic mice. *J. Leukocyte Biol.* **2007**, *81* (1), 100–107.
(41) Mannervick, B.; Alin, P.; Guthenberg, C.; Jensson, H.; Tahir, M. K.; Warholm, M.; Jornvall, H. Identification of three classes of cytosolic glutathione transferase enzymatic properties. *Proc. Natl. Acad. Sci. U.S.A.* **1985**, *82*, 7202–7206.
(42) Whalen, R.; Boyer, T. D. Human glutathione S-transferases. *Semin. Liver Dis.* **1998**, *18* (4), 345–358.
(43) Coles, B.; Ketterer, B. The role of glutathione and glutathione transferases in chemical carcinogenesis. *Crit. Rev. Biochem. Mol. Biol.* **1990**, *25*, 47–70.
(44) Tsuchida, S.; Sato, K. Glutathione transferases and cancer. *Crit. Rev. Biochem. Mol. Biol.* **1992**, *27*, 337–384.
(45) Rushmore, T. H.; Pichett, C. B. Glautathione S-transferases. Supergene family: regulation, and therapeutic implications. *J. Biol. Chem.* **1993**, *268*, 11475–11478.
(46) Hayes, J. D.; Pulford, D. J. The glutathione S-transferase supergene family: regulation of GST and the contribution of the isoenzymes to cancer chemoprotection and drug resistance. *Crit. Rev. Biochem. Mol. Biol.* **1995**, *30*, 445–600.
(47) Mohammadzadeh Ghobadloo, S.; Yaghmaei, B.; Allameh, A.; Hassani, P.; Noorinayer, B.; Zali, M. R. Polymorphisms of glutathione S-transferase M1, T1, and P1 in patients with HBV-related liver cirrhosis, chronic hepatitis, and normal carriers. *Clin. Biochem.* **2006**, *39* (1), 46–49.
(48) Yu, M. W.; Yang, S. Y.; Pan, I. J.; Lin, C. L.; Liu, C. J.; Liaw, Y. F.; Lin, S. M.; Chen, P. J.; Lee, S. D.; Chen, C. J. Polymorphisms in XRCC1 and glutathione S-transferase genes and hepatitis B-related hepatocellular carcinoma. *J. Natl. Cancer Inst.* **2003**, *95* (19), 1485–1488.
(49) Van Greevenbroek, M. M.; Vermeulen, V. M.; De Bruin, T. W. Identification of novel molecular candidates for fatty liver in the hyperlipidemic mouse model, HcB19. *J. Lipid Res.* **2004**, *45* (6), 1148–1154.
(50) Douette, P.; Navet, R.; Gerkens, P.; de Pauw, E.; Leprince, P.; Sluse-Goffart, C.; Sluse, F. E. Steatosis-induced proteomic changes in liver mitochondria evidenced by two-dimensional differential in-gel electrophoresis. *J. Proteome Res.* **2005**, *4* (6), 2024–2031.
(51) Siegers, C. P.; Bossen, K. H.; Younes, M.; Mahlke, R.; Oltmanns, D. Glutathione and glutathione-S-transferases in the normal and diseased human liver. *Pharmacol. Res. Commun.* **1982**, *14* (1), 61–72.
(52) Burim, R. V.; Canalle, R.; Martinelli Ade, L.; Takahashi, C. S. Polymorphisms in glutathione S-transferases GSTM1, GSTT1 and GSTP1 and cytochromes P450 CYP2E1 and CYP1A1 and susceptibility to cirrhosis or pancreatitis in alcoholics. *Mutagenesis* **2004**, *19* (4), 291–298.
(53) Ghobadloo, S. M.; Yaghmaei, B.; Bakayev, V.; Goudarzi, H.; Noorinayer, B.; Rad, F. H.; Samiy, S.; Aghabozorghi, S.; Zali, M. R. GSTP1, GSTM1, and GSTT1 genetic polymorphisms in patients with cryptogenic liver cirrhosis. *J. Gastrointest. Surg.* **2004**, *8* (4), 423–427.
(54) Lee, H. C.; Lee, H. S.; Jung, S. H.; Yi, S. Y.; Jung, H. K.; Yoon, J. H.; Kim, C. Y. Association between polymorphisms of ethanol-metabolizing enzymes and susceptibility to alcoholic cirrhosis in a Korean male population. *J. Korean Med. Sci.* **2001**, *16* (6), 745–750.
(55) Cichoz-Lach, H.; Partycka, J.; Nesina, I.; Celinski, K.; Slomka, M.; Wojcierowski, J. Alcohol dehydrogenase and aldehyde dehydrogenase gene polymorphism in alcohol liver cirrhosis and alcohol chronic pancreatitis among Polish individuals. *Scand. J. Gastroenterol.* **2007**, *42* (4), 493–498.
(56) Mori, T.; Nagai, K.; Mori, M.; Nagao, M.; Imamura, M.; Iijima, M.; Kobayashi, K. Progressive liver fibrosis in late-onset argininosuccinate lyase deficiency. *Pediatr. Dev. Pathol.* **2002**, *5* (6), 597–601.
(57) Bergeron, A.; D'Astous, M.; Timm, D. E.; Tanguay, R. M. Structural and functional analysis of missense mutations in fumarylacetoacetate hydrolase, the gene deficient in hereditary tyrosinemia type 1. *J. Biol. Chem.* **2001**, *276* (18), 15225–15231.
(58) Taketa, K.; Shimamura, J.; Takesue, A.; Tanaka, A.; Kosaka, K. Undifferentiated patterns of key carbohydrate-metabolizing enzymes in injured livers. II. Human viral hepatitis and cirrhosis of the liver. *Enzyme* **1976**, *21* (3), 200–210.
(59) Sutton, A.; Nahon, P.; Pessayre, D.; Rufat, P.; Poiré, A.; Ziol, M.; Vidaud, D.; Barget, N.; Ganne-Carrié, N.; Charnaux, N.; Trinchet, J. C.; Gattegno, L.; Beaugrand, M. Genetic polymorphisms in antioxidant enzymes modulate hepatic iron accumulation and hepatocellular carcinoma development in patients with alcohol-induced cirrhosis. *Cancer Res.* **2006**, *66* (5), 2844–2852.
(60) Seckin, Y.; Harputluoglu, M. M.; Batcioglu, K.; Karincaoglu, M.; Yildirim, B.; Oner, R. I.; Uyumlu, B.; Aydogdu, N.; Hilmioglu, F. Gastric tissue oxidative changes in portal hypertension and cirrhosis. *Dig. Dis. Sci.* **2007**, *52* (5), 1154–1158.
(61) Czeczot, H.; Scibior, D.; Skrzycki, M.; Podsiad, M. Activity of antioxidant enzymes in patients with liver cirrhosis. *Wiad. Lek.* **2006**, *59* (11−12), 762–766.
(62) Spitsyn, V. A.; Nafikova, A. Kh.; Spitsyna, N. Kh.; Afanas'eva, I. S. Genetic predisposition to development of toxic liver cirrhosis caused by alcohol. *Genetika* **2001**, *37* (5), 698–707.
(63) Yamaguchi, M.; Isogai, M.; Shimada, N. Potential sensitivity of hepatic specific protein regucalcin as a marker of chronic liver injury. *Mol. Cell. Biochem.* **1997**, *167* (1−2), 187–190.

PR7006522